Check for updates

physica status solidi (a)

RESEARCH ARTICLE OPEN ACCESS

Time-Resolved Photoluminescence Lifetime Measurements of Organic Photovoltaic Materials

Levente Illés[1,2] | Ferenc Steinbach[1,2] | Ferenc Korsós[2] | Tamás Brigancz[2] | Attila Barócsi[1] | Alexandros Zachariadis[3] | Christos Kapnopoulos[3] | Evangelos Mekeridis[4] | Argiris Laskarakis[3] | Stergios Logothetidis[4] | Zoltán Tamás Kiss[2] | Sándor Lenk[1]

[1]Department of Atomic Physics, Institute of Physics, Budapest University of Technology and Economics, Budapest, Hungary | [2]Semilab Semiconductor Physics Laboratory Co. Ltd., Budapest, Hungary | [3]Nanotechnology Lab LTFN, Department of Physics, Aristotle University of Thessaloniki, Thessaloniki, Greece | [4]Organic Electronic Technologies P.C. (OET), Thermi, Thessaloniki, Greece

Correspondence: Levente Illés (levente.illes@semilab.hu)

Received: 10 October 2025 | **Revised:** 31 January 2026 | **Accepted:** 26 February 2026

Keywords: fluorescence lifetime | organic semiconductor | time-correlated single photon counting

ABSTRACT

This research investigates organic photovoltaic (OPV) structures using time-correlated single photon counting (TCSPC) to study time-resolved fluorescence dynamics under low injection conditions. A picosecond laser diode with a wavelength of 650 nm and a single photon avalanche diode (SPAD) are applied for excitation and detection. The measurements are performed at an irradiance of 0.011 W/cm^2 (1.2×10^8 photons/pulse) which is sufficiently low to avoid damaging the sample. Decay characteristics are analyzed using iterative reconvolution. The samples include various absorber species and structural configurations, revealing fluorescence decay components as short as 30–500 ps. Such rapid dynamics can only be detected using conventional photodiode-based setups at much higher excitation levels. The findings indicate that while absorption spectra vary with structural properties like layer thickness, decay times are primarily determined by the absorber material. TCSPC measurements thus provide deeper insights into the recombination dynamics of organic semiconductors.

1 | Introduction

Light can be converted to electric current through the photoelectric effect, which can then be utilized in numerous ways. Although this phenomenon was discovered nearly two centuries ago by Becquerel, its applications have only multiplied over time [1]. Today, photovoltaic structures are integral components of various devices such as measurement instruments, motion sensors, mobile phones, and solar panels. Initially, the solar industry focused on using monocrystalline or multicrystalline silicon in an attempt to maximize the efficiency of solar cells [2, 3]. By the late 20th century, the rise of nanotechnology led to the development and exploration of alternative photovoltaic thin-film structures and their physical properties.

The first silicon-based solar cell was developed in 1954 at Bell Laboratories, achieving an efficiency of only 6% [4]. Currently, the highest efficiency for a silicon-based heterojunction (SHJ) solar cell has reached 27.3% [5], approaching the theoretical maximum of 30% calculated by W. Shockley and H. J. Queisser, according to their bandgap calculations [6].

The solar cell industry focuses on three key aspects: increasing efficiency, reducing production costs, and ensuring sustainable raw material supply. Since the efficiency of silicon-based solar cells is nearing their theoretical limit, reducing manufacturing costs presents a viable strategy for these cells. Another development direction involves researching new layer structures with higher efficiency and improving production technologies. Although these advancements are costly in the research phase, many companies and research institutes pursue them with the expectation of lower future production costs and higher efficiency. Novel structures include perovskite-based cells, copper-

This is an open access article under the terms of the Creative Commons Attribution License, which permits use, distribution and reproduction in any medium, provided the original work is properly cited.

© 2026 The Author(s). *physica status solidi (a)* applications and materials science published by Wiley-VCH GmbH.

indium-gallium-selenide (CIGS), TiO_2 solar cells, and organic solar cells (OSCs) [7–11].

The first electrically conducting organic polymers were developed by Shirakawa and colleagues in 1977 [12], laying the foundation for the development of the first organic semiconductors, transistors, and solar cells. The electronic properties of organic photovoltaic (OPV) devices are determined by the electron structure of carbon molecules, combined with other atoms like oxygen and hydrogen.

OPVs can be classified based on the number of components they contain as either single-component (homojunction solar cells) or multicomponent (heterojunction solar cells). A heterojunction OSC consists of two components, referred to as the electron donor (D) and electron acceptor (A). Depending on the geometric structure of the heterojunction OSC, there are planar and bulk configurations. In planar heterojunction OSCs, the donor and acceptor layers are deposited sequentially onto a substrate. In contrast, bulk heterojunction OSCs form an irregular structure by mixing the donor and acceptor materials together [13].

The energy structures of the OSCs mostly have been described using molecular orbital (MO) theory. Electrons tend to occupy the lowest energy molecular state, stabilizing the molecular chain. The highest energy level occupied by an electron is termed as the highest occupied molecular orbital (HOMO), while the lowest unoccupied energy state is referred to as the lowest unoccupied molecular orbital (LUMO, Figure 1).

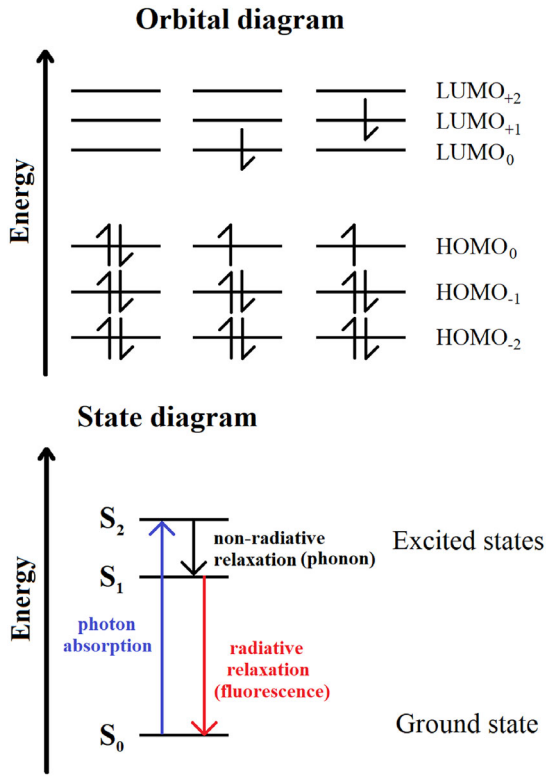

FIGURE 1 | Orbital diagram with HOMO and LUMO levels (top). State diagrams (bottom) with excited singlet states (S_1 as $LUMO_0$ and S_2 as $LUMO_{+1}$) and ground state (S_0 as $HOMO_0$) showing the photon absorption (blue), nonradiative relaxation (black), and radiative relaxation (red) events.

Upon a photon excitation in OSCs, excitons are generated following photon absorption. An exciton is a particle-like mobile energy concentration consisting of an electron–hole pair, held together by Coulombic interaction temporarily without recombination. Excitons can be formed in both the donor (D) and acceptor (A) layers and are associated with a characteristic lifetime (τ_{ex}). In an optimally designed OSC, excitons diffuse to the D–A interface within their lifetime, where they are dissociated into free charge carriers. For efficient current generation, it is crucial that the excitons reach the interface before they collapse within this process determined by their lifetime and diffusivity (D).

$$L_D = \sqrt{D\tau_{ex}} \tag{1}$$

The L_D diffusion length limits planar heterojunction OSCs, as if the D or A layer thickness exceeds this distance, charge separation occurs only for excitons created within the distance L_D of the interface [14]. Conversely, if the layer thickness is too small, photon absorption decreases, reducing the number of excitons and thus lowering the OSC efficiency. In contrast, in bulk heterojunction solar cells the diffusion length does not limit the thickness of the absorber layer, yet it remains a critical parameter during the preparation of the active layer. One of the key factors in achieving high efficiency is the alignment of the diffusion length with the characteristic size of the resulting domains [15].

After charge separation, three scenarios may occur. In the first case, the electron–hole pair exits the absorber through diffusion via the electron transport layer (ETL) and hole transport layer (HTL). The other two scenarios are called geminate and nongeminate recombination (GR and NGR) processes, respectively. In case of GR, the electron–hole pair originates from a monomolecular process, while in NGR, an electron and hole from different excitons recombine [16]. Both recombination processes result in photon emission but occur on different timescales. In case of GR, photon emission occurs at a sub-nanosecond timescale [17], in contrast to NGR which has a lifetime of 10–1000 ns.

The photoluminescence (PL) signal itself contains information about the physical properties of the sample under investigation, such as band structure, morphology, and composition. However, to effectively excite the sample, it is essential to know its absorption spectra, i.e., the wavelengths at which it can absorb more photons, which can be characterized using a UV–VIS spectrometer equipped with an integration sphere to account for scattering of the thin film.

In the simple case where relaxation proceeds exclusively through photon emission, the number of excited molecules is proportional to the number of emitted photons. By measuring the temporal evolution of the light intensity, one can therefore determine the duration for which a given molecule or molecular ensemble remains in the excited state. If the excitation is treated as a Dirac delta function, the resulting intensity curve can be approximated by an exponentially decaying function, whose exponent contains the parameter τ_{PL} referred to as PL lifetime. The intensity profile can be described by a single exponential function. In more complex systems, when the PL decay can't be described by a single exponential function, this simple approximation is no longer applicable. Furthermore, in some cases the excitation pulse cannot be treated as a Dirac delta function relative to the decay timescale. In this case, data evaluation requires a different approach, such as the iterative reconvolution discussed later.

18626319, 2026, 8, Downloaded from https://onlinelibrary.wiley.com/doi/10.1002/pssa.202500868 by Cochrane Hungary, Wiley Online Library on [21/04/2026]. See the Terms and Conditions (https://onlinelibrary.wiley.com/terms-and-conditions) on Wiley Online Library for rules of use; OA articles are governed by the applicable Creative Commons License

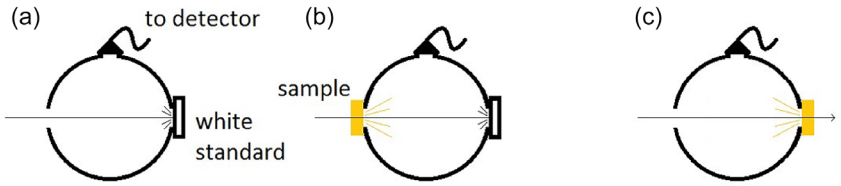

FIGURE 2 | Geometry of calibration (a), total transmittance (b), and reflectance (c) measurements [28].

The phenomenon of PL is illustrated using the state diagram (Figure 1). In this process, photon absorption forces the molecules to reach a higher energy state (S1 or S2, excited state). The absorbed photon energy can then be released by the molecule through either radiative way (radiative relaxation) or nonradiative way (NR relaxation). In the first case, the excitation results in the emission of a photon whose energy corresponds to the difference between the S_1 and S_0 energy states, while in the second case, the remaining energy is dissipated in the form of lattice vibrations (phonons) and other NR processes.

The components characterizing the PL decay of OSC are given by the diffusion equation for excitons [18]

$$\frac{dn(t,\vec{r})}{dt} = D\nabla^2 n(t,\vec{r}) + G(t) - (k_{\text{rad}} + k_{\text{nrad}})n(t,\vec{r}) \quad (2)$$

where k_{rad} and k_{nrad} represent the rate of all radiative and NR relaxation processes, respectively.$n(t,\vec{r})$ is the number of excitons, D is the diffusion constant, $G(t)$ is the number of generated excitons, t is the time, and ∇^2 is the Laplace operator. This simple model does not account for exciton–exciton annihilation, where the collision of two excitons leads to their mutual quenching, an effect that cannot be described by a first-order term. In more complex models, we encounter a form of the equation that includes this effect, thus expanding with a decay term $\Gamma n^2(t,\vec{r})$, however, this term becomes significant only at high excitation cases [19–22]. Consequently, the transient PL signal from photon excitation consists of multiple components, and detailed analysis of these provides insights into the recombination processes in OSC samples.

Transient PL measurements have been successfully applied to OPV blends to monitor the ultrafast conversion of singlet excitons into charge-transfer states and to quantify the respective contributions of static and dynamic energetic disorder [23]. Sub-nanosecond decay times can be measured using fast photon detectors and oscilloscopes. However, this requires high-energy excitation; otherwise, the PL signal may be small comparable to the detector noise. When working with low-energy excitations, an alternative measurement technique is necessary to measure short decay times effectively. Time-correlated single photon counting (TCSPC) is a suitable technique for determining decay times within this time range for various photoluminescent samples, such as biological tissues, semiconductor nanostructures, and colloidal quantum dots [24, 25]. TCSPC measurements also allow us to observe significant lifetime differences between excitons and longer-lived excited states. By characterizing these emission signatures, it becomes possible to determine key parameters such as quasi-Fermi-level splitting and carrier-related losses, as demonstrated in recent studies [26, 27].

This measurement principle involves measuring the time interval between the emission of an excitation photon and the arrival of the first emitted photon at the detector using a time-stamping technique. The system assigns the detected photon to the appropriate time bin and, by repeating the excitation, a histogram of photon arrival is generated [23]. This photon statistics represents the decay of the sample, typically modeled by fitting a sum of exponential functions depending on the physical processes triggered by the excitation. The fitting parameters are used to calculate an intensity-averaged lifetime, which characterizes the transient processes within the sample and gives a good reproducible time constant. In this study, we aim to measure decay components in the picosecond- and nanosecond-range and to analyze the information they provide about the sample's physical and dynamical properties.

2 | Materials and Methods

2.1 | Spectral Measurements

The transmission and reflection spectra of the samples were measured using a spectrometer (LAMBDA 1050, PerkinElmer).

The spectrometer contains an integrating sphere module that gives the possibility to measure transmittance and reflectance spectra including forward and backward scattered light, respectively. The range of spectral measurements was set from 400 to 850 nm with a slit width of 4 nm, scan speed of 156 nm/min and step size of 5 nm. For the calibration and the transmission measurements a white standard (PerkinElmer Spectralon) with high diffuse reflectance has been used (Figure 2).

In case of a reflective sample the absorbance is defined as

$$A = -\log(R+T) \quad (3)$$

where T is the total transmittance and R is the reflectance of the sample at a specified wavelength.

2.2 | TCSPC Technique

The basis of the measurement setup used here has been described in detail in [29] and shown in Figure 3. Briefly, a picosecond, 650 nm fiber-coupled diode laser (LDH-P-C-650, PicoQuant) provides excitation, with parameters adjusted to optimize pulse shape and fluorescence decay capture (1.2×10^8 photons/pulse, 10 MHz repetition rate). A single-mode fiber and collimator produce a Gaussian beam (2.04 mm diameter). The exact positioning of the laser beam is done by a mirror, with the incidence angle set to 30°, which spatially separates the excitation from the specular reflection. Both the specular reflected and transmitted light are absorbed by light traps. The PL photons are collected by a further optimized imaging optic consisting of two achromatic lenses (#49-321 and #49-323, Edmund Optics). A long-pass filter

18626319, 2026, 8, Downloaded from https://onlinelibrary.wiley.com/doi/10.1002/pssa.202500868 by Cochrane Hungary, Wiley Online Library on [21/04/2026]. See the Terms and Conditions (https://onlinelibrary.wiley.com/terms-and-conditions) on Wiley Online Library for rules of use; OA articles are governed by the applicable Creative Commons License

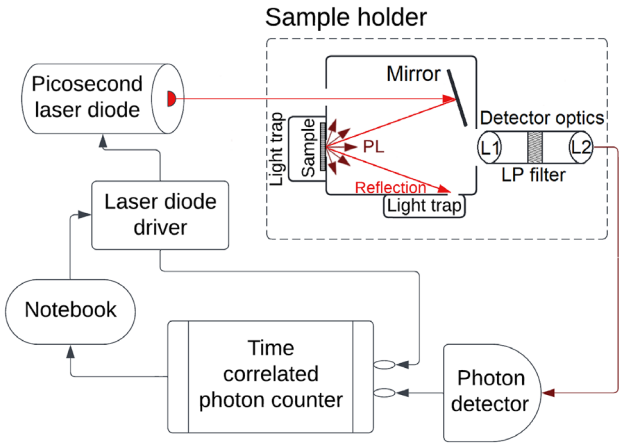

FIGURE 3 | Scheme of TCSPC measurement setup.

(#66-226, Edmund Optics) is placed between these lenses in the collimated beam, which has a cut-on wavelength of 750 nm and separates the remaining excitation photons from the fluorescent photons. Collected photons are guided via a multimode fiber (M129L01, Thorlabs) to a single-photon avalanche diode (PDM-100-CTB, Micro Photon Devices). The photon events were registered by time-tagger electronics (PicoHarp 300, PicoQuant) with 4 ps time bins.

Typically, the photon histograms of the OPV samples include lifetime components below 100 ps, which is comparable to the full width at half maximum (FWHM) of the instrument response function (IRF). As a result, the IRF alters the obtained photon statistics, leading to a significant decrease in fitting quality and affecting the overall result. This issue can be reduced by employing the iterative reconvolution method for fitting [30]. To achieve this, the IRF of the system must be measured, e.g., by placing a diffuse scattering reference sample in the sample position and measuring the scattered light without the long-pass filter. The data evaluation is carried out by the Easy Tau 2 (PicoQuant) software. During iterative reconvolution, this IRF is convolved with a predefined function type, which is a three-component multiexponential function ($N = 3$) with time constants τ_n and amplitudes A_n (Equation (4)). The result of the convolution is then compared by the software to the decay curve, and the fitting parameters are adjusted to minimize the difference. The so-called χ^2 parameter has been used to quantify this difference between convolution and decay [30]. The samples are finally characterized by intensity-averaged lifetimes (τ_{Avg}).

$$f(t) = \sum_{n=1}^{N} A_n e^{-\frac{t}{\tau_n}} \tag{4}$$

$$\tau_{\mathrm{Avg}} = \frac{\sum_{n=1}^{N} A_n \tau_n^2}{\sum_{n=1}^{N} A_n \tau_n} \tag{5}$$

2.3 | OPV Samples

The organic semiconductor samples used in the measurements were provided by the Aristotle University of Thessaloniki. Five different types of absorber layers were examined, which will be referred to as A, B, C, D, and E in the following discussion. Absorber A corresponds to an OET-D1:A1-type material (polymer donor D1 with a fullerene-based acceptor A1), while Absorber B corresponds to an OET-D2:A2-type material (polymer donor D2 with a fullerene-based acceptor A2). Absorber C consists of PPDT2FBT:PC60BM (polymer donor PPDT2FBT with the fullerene-based acceptor PC60BM), Absorber D consists of PPDT2FBT:Y5 (polymer donor PPDT2FBT with the nonfullerene-based acceptor Y5), and Absorber E consists of PM6:Y7 (polymer donor PM6 with the nonfullerene-based acceptor Y7).

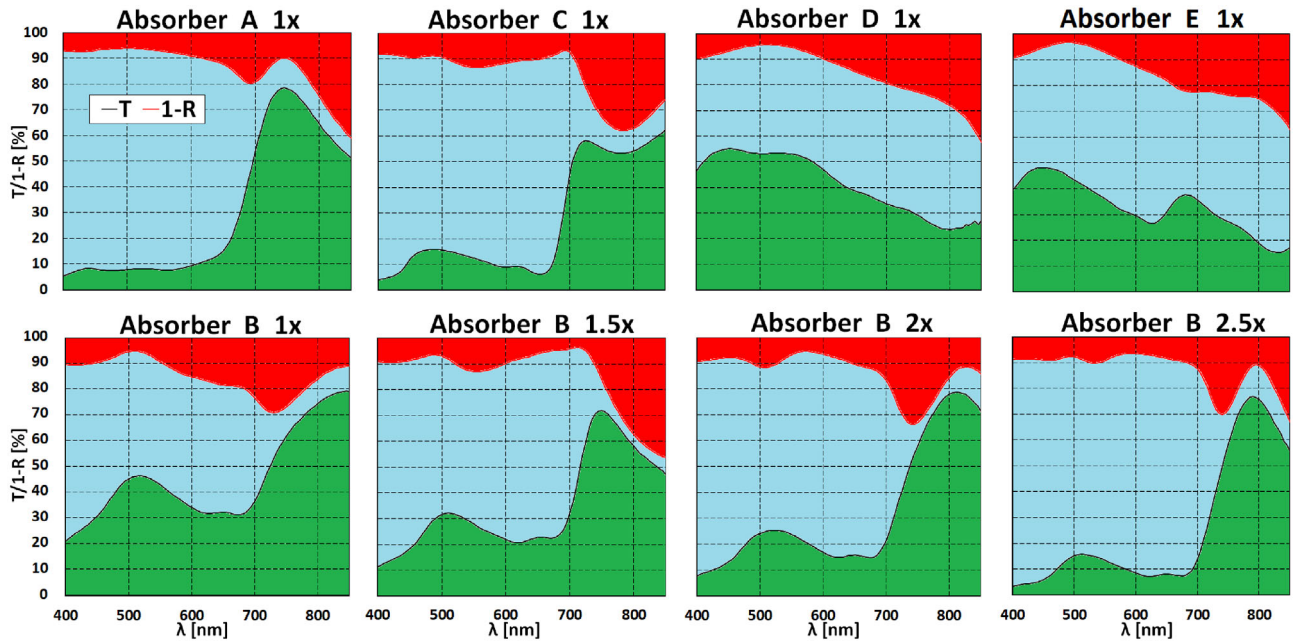

FIGURE 4 | Transmission (green) and 1-reflection (red) spectra of the samples. A, C, D, and E absorber layers (top) and B type absorber at different layer thicknesses (bottom). In between the green and red regions, the blue region represents the degree of the absorption at the given wavelength.

18626319, 2026, 8, Downloaded from https://onlinelibrary.wiley.com/doi/10.1002/pssa.202500868 by Cochrane Hungary, Wiley Online Library on [21/04/2026]. See the Terms and Conditions (https://onlinelibrary.wiley.com/terms-and-conditions) on Wiley Online Library for rules of use; OA articles are governed by the applicable Creative Commons License

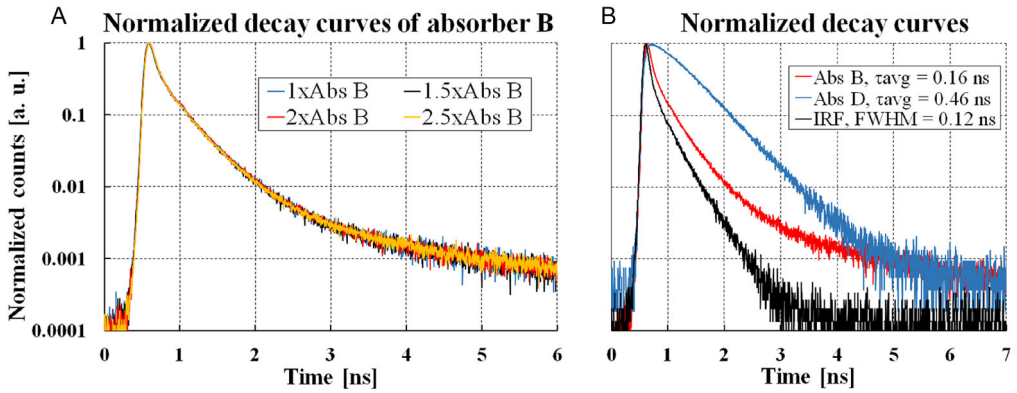

FIGURE 5 | Normalized decay curves of Absorber B at different thicknesses (A) and those of Absorber B, Absorber D, and the IRF (B). The calculated intensity-averaged lifetimes and the FWHM of the IRF are provided in the figure legend.

The exact materials of Absorber A and B are confidential information, but they are similar to the examples described in previous publications [31, 32].

The thicknesses of the absorber layers varied among samples, with each being referenced relative to the thinnest layer. These thickness variations were labeled as 1x, 1.5x, 2x, and 2.5x, where "x" represents the thinnest layer ($x \approx 200$ nm based on reflectometry measurements), and the preceding number indicates the multiplication factor. Additionally, for the sample labeled B, we investigated whether the ETL (SnO) applied to the sample influenced the decay times. All samples were equipped with a HTL (PEDOT:PSS) as well. A total of 14 samples were tested. The samples had dimensions of $80\,\text{mm} \times 20\,\text{mm} \times 0.1$ mm. Measurements were carried out at three different locations on each sample, since inhomogeneities are present due to the Slot Die coating manufacturing process. The averages of the intensity-averaged lifetimes were assigned as lifetimes for the given sample, the measurement errors were calculated from the statistical standard deviation.

3 | Results and Discussion

3.1 | Spectral Response

Comparing both transmission and reflection spectra of the samples, the absorption begins to increase below 750 nm and occurs between 400 and 700 nm with varying efficiency. (Figure 4 top row). Absorption increases with thickness, as shown in the bottom row of Figure 4 for Absorber B. However, this measurement confirms a deviation from the given thickness values. The absorption spectra confirm that all the OPV samples can be excited at 650 nm. Although, D and E samples show lower absorption values across the entire visible spectrum, the scale of absorption was sufficient for TCSPC measurements.

3.2 | Decays of Organic Photovoltaic Samples

The measured intensity-averaged lifetimes ranged between 0.16 and 0.46 ns as shown in the normalized decay curves in Figure 5B, presented alongside the IRF measurement. For absorber layers of the same type, variations in thickness affected the sum of the detected emission photon counts. The relationship between thickness and either peak signal intensity or total photon count is nonlinear; however, thinner layers consistently exhibit lower peak photon counts. When normalizing the decay curves to these maximum values, it is evident that the decay time constant is an invariant quantity regardless of thickness (Figure 5A).

Iterative reconvolutions with the sum of three exponential functions were carried out for all the samples independently. Calculating the mean and standard deviation of the obtained fitting parameters reveals regular patterns. The resulting τ_1, τ_2, and τ_3 parameters do not significantly deviate among identical types of absorber layers (Table 1), but differences can be observed between different materials. It should be noted that the exact value of the shortest component also varies between absorber materials, indicating that the shortest lifetime component also contains a material-dependent response. The absorber B sample

TABLE 1 | Average and standard deviation values of the fitted fluorescence lifetime parameters of samples A to E with different absorber layer thicknesses. For sample details, please refer to the text.

Sample	τ_1, ps	τ_2, ps	τ_3, ps
A_1x	1457 ± 27	327 ± 4	31 ± 1
A_1.5x	1458 ± 22	338 ± 2	35 ± 1
B_1x	1617 ± 14	280 ± 2	29 ± 0.4
B_1.5x	1699 ± 57	287 ± 3	28 ± 0.5
B_2x	1775 ± 35	295 ± 2	28 ± 1
B_2.5x	1789 ± 36	298 ± 2	28 ± 0.2
B_1x_ETL	1778 ± 39	300 ± 3	27 ± 1
B_1.5x_ETL	1934 ± 90	305 ± 7	26 ± 1
B_2x_ETL	1769 ± 15	291 ± 2	26 ± 0.3
B_2.5x_ETL	1815 ± 19	295 ± 2	26 ± 0.3
C_1x	2303 ± 269	308 ± 10	28 ± 5
C_1.5x	2088 ± 28	294 ± 11	27 ± 0.2
D_1x	1473 ± 153	459 ± 6	73 ± 1
D_2.5x	1255 ± 49	454 ± 16	99 ± 5
E_1x	1611 ± 36	341 ± 17	26 ± 4
E_1.5x	1754 ± 107	358 ± 7	17 ± 5

18626319, 2026, 8, Downloaded from https://onlinelibrary.wiley.com/doi/10.1002/pssa.202500868 by Cochrane Hungary, Wiley Online Library on [21/04/2026]. See the Terms and Conditions (https://onlinelibrary.wiley.com/terms-and-conditions) on Wiley Online Library for rules of use; OA articles are governed by the applicable Creative Commons License

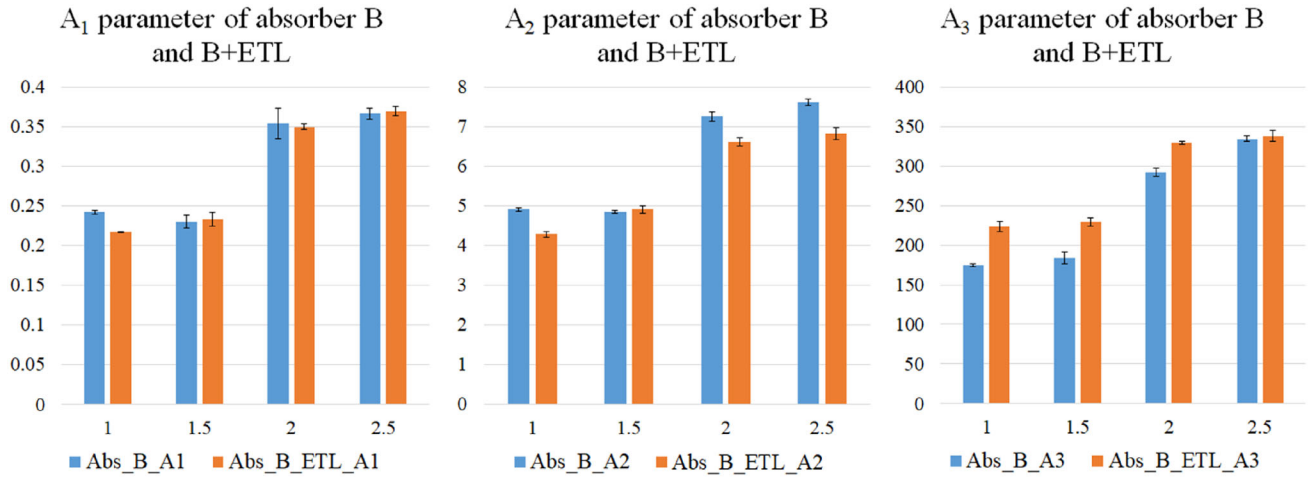

FIGURE 6 | Weight parameters of Absorber B and B + ETL depending on the layer thickness.

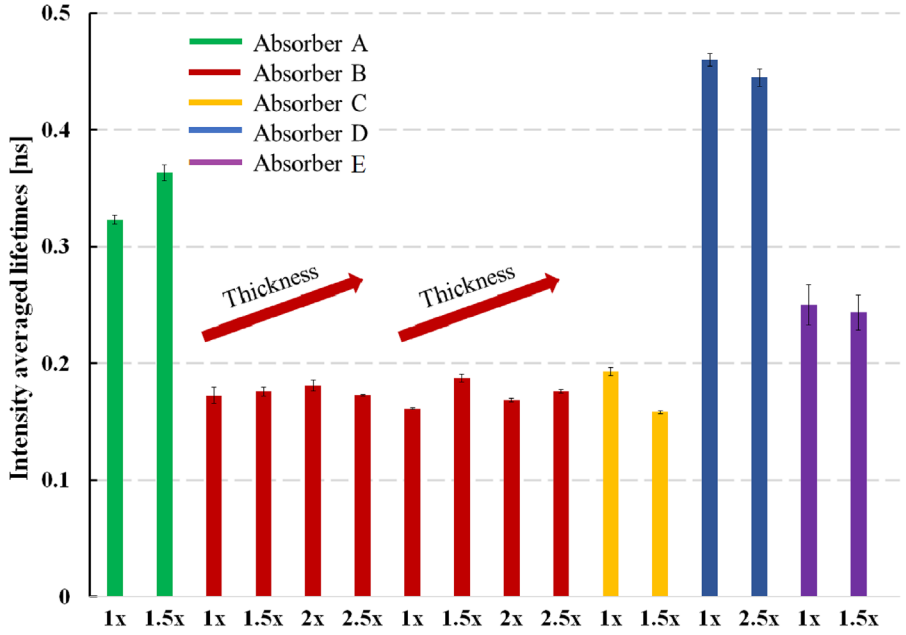

FIGURE 7 | Intensity-averaged lifetimes of the OPV samples. Absorber layers of the same type are marked by the same color.

was tested with and without the ETL, and its presence did not influence the calculated lifetime components.

It is observed that for samples of the same material, the weights of the time constants (A_1, A_2, A_3) vary with the thickness, which can be explained by the correlation between PL signal intensity and layer thickness. The weights of the time constants are presented for absorber B with different thicknesses, both with and without ETL layer, in Figure 6. The shortest lifetime component (τ_3), which is less than 100 ps, has the highest weight among the components (τ_1, τ_2, τ_3) in all cases. This short component can only be determined using the iterative reconvolution method. Using this approach lifetime components equivalent to a tenth of the FWHM of the IRF have been reported [33, 34]. The observed decay curves provide material-specific characteristics of the excited state dynamics. Therefore, the intensity-averaged lifetime proves to be an effective parameter for comparing the decay properties of different material systems.

The intensity-averaged lifetime can be used as a comparative parameter to distinguish the recombination dynamics of different absorber blends, as it exhibits characteristic values for each material system. Notably, sample inhomogeneities do not lead to significant variations in the decay curves, as indicated by the relatively small error bars (Figure 7). The "B" and "C" layers exhibited values between 0.16 and 0.2 ns, while the "A" type layer had significantly longer lifetimes, ranging from 0.3 to 0.4 ns. The longest decay was observed in the "D" layer, with values exceeding 0.4 ns (Figure 7). The intensity-averaged lifetime for the same type of absorber layers does not change with increasing thickness or the presence of an ETL.

4 | Conclusion

The primary objective of this research has been to investigate photoluminescent decay profiles of different OPV blends and

18626319, 2026, 8, Downloaded from https://onlinelibrary.wiley.com/doi/10.1002/pssa.202500868 by Cochrane Hungary, Wiley Online Library on [21/04/2026]. See the Terms and Conditions (https://onlinelibrary.wiley.com/terms-and-conditions) on Wiley Online Library for rules of use; OA articles are governed by the applicable Creative Commons License

to characterize them by the intensity-averaged lifetime. The measurements have been conducted at low irradiance, allowing for a nondestructive analysis using this measurement technique. The absorption spectrum of the investigated samples varies depending on their material and increases with thickness.

The results indicate a correlation between the intensity-averaged lifetimes and the molecular species of the absorber layers within the organic samples. Additionally, the data suggest that the relative thickness of the absorber layer does not significantly affect the lifetimes, but it does correlate with the weight of the lifetime parameters and PL intensity.

Another key observation is that the decay in all samples can be accurately described using a multiexponential function consisting of three components. The sub-nanosecond intensity-averaged lifetime calculated from the fits indicates that the shortest component in all samples is under 100 ps. The high weight of this component suggests that rapid relaxation processes, likely associated with GR at the donor–acceptor interface or efficient exciton quenching play a major role. The intermediate τ_2 component falls within the sub-ns regime, consistent with the typical radiative lifetime of bound charge transfer states. Finally, the longest lifetime parameter τ_3 appears as a low-amplitude tail, characteristic of delayed emission indicative of trap-assisted recombination processes.

In conclusion, characterizing fast recombination mechanisms such as GR plays a crucial role in understanding the material properties of these OPV blends. To measure such a short lifetime component, using sub-nanosecond pulses and the iterative reconvolution-based data analysis is mandatory.

Author Contributions

Levente Illés: methodology (lead), project administration (lead), visualization (lead), writing – original draft (lead). **Ferenc Steinbach**: formal analysis (supporting), visualization (supporting). **Ferenc Korsós**: formal analysis (supporting), supervision (supporting), visualization (supporting). **Tamás Brigancz**: conceptualization (equal), supervision (equal). **Attila Barócsi**: conceptualization (equal), supervision (equal), writing – review & editing (equal). **Alexandros Zachariadis**: resources (lead). **Christos Kapnopoulos**: resources (equal). **Evangelos Mekeridis**: resources (supporting). **Argiris Laskarakis**: resources (equal), writing – review & editing (equal). **Stergios Logothetidis**: resources (equal), writing – review & editing (equal). **Zoltán Tamás Kiss**: project administration (equal). **Sándor Lenk**: conceptualization (lead), supervision (lead), writing – original draft (equal), writing – review & editing (lead).

Acknowledgments

The authors thank the Nanotechnology Laboratory, Aristotle University of Thessaloniki, for providing the OPV samples.

Funding

This study was supported by the Ministry of Culture and Innovation of Hungary from the National Research, Development and Innovation Fund (Project No. KDP-IKT-2023-900-I1-00000957/0000003 under the KDP-2023 funding scheme, and Project No. 2022-2.1.1-NL-2022-00004), and HORIZON EUROPE Framework Programme (101096803 — Flex2Energy — HORIZON-CL5-2022-D3-01). S. L. was supported by the János Bolyai Research Scholarship of the Hungarian Academy of Sciences (BO/00038/23/11).

Conflicts of Interest

The authors declare no conflicts of interest.

Data Availability Statement

All data that support the findings of this study are included within the article (and any supplementary files).

References

1. A. Goetzberger, C. Hebling, and H.-W. Schock, "Photovoltaic materials, history, status and outlook," *Materials Science and Engineering: R: Reports* 40 (2003): 1–46.

2. A. Richter, M. Hermle, and S. W. Glunz, "Reassessment of the Limiting Efficiency for Crystalline Silicon Solar Cells," *IEEE Journal of Photovoltaics* 3 (2013): 1184–1191.

3. A. Bosio, S. Pasini, and N. Romeo, "The History of Photovoltaics with Emphasis on CdTe Solar Cells and Modules," *Coatings* 10, no. 4 (2020): 344.

4. A. Goetzberger, J. Luther, and G. Willeke, "Solar Cells: Past, Present, Future," *Solar Energy Materials & Solar Cells* 74 (2002): 1–11.

5. J. Yang, Y. Tong, C. Zhou, et al., "Unveiling the Mechanism of Ultraviolet-Induced Degradation in Silicon Heterojunction Solar Cells," *Solar Energy Materials and Solar Cells* 276 (2024): 113062.

6. W. Shockley and H. J. Queisser, "Detailed Balance Limit of Efficiency of p-n Junction Solar Cells," *Journal of Applied Physics* 32 (1961): 510–519.

7. M. A. Green and A. Ho-Baillie, "Perovskite Solar Cells: The Birth of a New Era in Photovoltaics," *ACS Energy Letters* 2 (2017): 822–830.

8. H. W. Schock and R. Noufi, "CIGS-Based Solar Cells for the Next Millennium," *Progress in Photovoltaics: Research and Applications* 8 (2000): 151–160.

9. A. Hagfeldt and M. Grätzel, "Light-Induced Redox Reactions in Nanocrystalline Systems," *Chemical Reviews* 95 (1995): 49–68.

10. Y. Liu, A. Hagfeldt, X. R. Xiao, and S. E. Lindquist, "Investigation of Influence of Redox Species on the Interfacial Energetics of a Dye-Sensitized Nanoprous TiO_2 Solar Cell," *Solar Energy Materials and Solar Cells* 55 (1998): 267–281.

11. G. A. Chamberlain, "Organic Solar Cells: A Review," *Solar Cells* 8 (1983): 47–83.

12. H. Shirakawa, E. J. Louis, A. G. MacDiarmid, C. K. Chiang, and A. J. Heeger, "Synthesis of Electrically Conducting Organic Polymers: Halogen Derivatives of Polyacetylene, (CH)x," *Journal of the Chemical Society, Chemical Communications* no. 16 (1977) : 578–580.

13. N. S. Sariciftci, D. Braun, C. Zhang, et al., "Semiconducting Polymer-Buckminsterfullerene Heterojunctions: Diodes, Photodiodes, and Photovoltaic Cells," *Applied Physics Letters* 62 (1993): 585–587.

14. M. T. Sajjad, A. Ruseckas, and I. D. W. Samuel, "Enhancing Exciton Diffusion Length Provides New Opportunities for Organic Photovoltaics," *Matter* 3 (2020): 341–354.

15. S. Mukherjee, C. M. Proctor, G. C. Bazan, T. Q. Nguyen, and H. Ade, "Significance of Average Domain Purity and Mixed Domains on the Photovoltaic Performance of High-Efficiency Solution-Processed Small-Molecule BHJ Solar Cells," *Advanced Energy Materials* 5 (2015): 1500877.

16. T. Hahn, S. Tscheuschner, F.-J. Kahle, et al., "Monomolecular and Bimolecular Recombination of Electron-Hole Pairs at the Interface of Bilayer Organic Solar Cell," *Advanced Functional Materials* 27 (2017): 1604906.

17. C. M. Proctor, M. Kuik, and T. Q. Nguyen, "Charge Carrier Recombination in Organic Solar Cells," *Progress in Polymer Science* 38 (2013): 1941–1960.

18626319, 2026, 8, Downloaded from https://onlinelibrary.wiley.com/doi/10.1002/pssa.202500868 by Cochrane Hungary, Wiley Online Library on [21/04/2026]. See the Terms and Conditions (https://onlinelibrary.wiley.com/terms-and-conditions) on Wiley Online Library for rules of use; OA articles are governed by the applicable Creative Commons License

18. E. M. Y. Lee and W. A. Tisdale, "Determination of Exciton Diffusion Length by Transient Photoluminescence Quenching and Its Application to Quantum Dot Films," *The Journal of Physical Chemistry C* 119 (2015): 9005–9015.

19. O. P. Dimitriev, "Dynamics of Exciton in Conjugated Molecules and Organic Semiconductor Systems," *Chemical Reviews* 122 (2022): 8487–8593.

20. O. V. Mikhnenko, P. W. M. Blom, and T. Q. Nguyen, "Exciton Diffusion in Organic Semiconductors," *Energy Environmental Science* 8 (2015): 1867–1888.

21. H. Wang, H. Y. Wang, B. R. Gao, et al., "Exciton Diffusion and Charge Transfer Dynamics in Nano Phase-Separated P3HT/PCBM Blend Films," *Nanoscale* 3 (2011): 2280–2285.

22. Y. Firdaus, V. M. L. Corre, S. Karuthedath, et al., "Long-Range Exciton Diffusion in Molecular Non-Fullerene Acceptors," *Nature Communications* 11, no. 1 (2020): 5220.

23. F.-J. Kahle, A. Rudnick, S. Wedler, et al., "Static and Dynamic Disorder of Charge Transfer States Probed by Optical Spectroscopy," *Advanced Energy Materials* 12 (2022): 2103328.

24. P. Kapusta, M. Wahl, and R. Erdmann, eds., *Advanced Photon Counting: Applications, Methods, Instrumentation*, Springer Series on Fluorescence, 15 (Springer, 2015).

25. J. R. Lakowicz, *Principles of Fluorescence Spectroscopy* (Springer, 2006).

26. M. List, J. Faisst, F. Heinz, and U. Würfel, "Determination of Free Charge Carrier Luminescence and Quasi-Fermi Level Separation in Organic Solar Cells via Transient Photoluminescence Measurements," *Advanced Optical Materials* 11 (2023): 2202213.

27. J. Faisst, M. List, C. Baretzky, A. W. Bett, and U. Würfel, "Implied Voltage and Current Characterization in Organic Solar Cells Using Transient Photoluminescence," *Advanced Energy Materials* 15 (2025): 2403881.

28. F. Galeotti, W. Mróz, M. Catellani, B. Kutrzeba-Kotowska, and E. Kozma, "Tailorable Perylene-Loaded Fluorescent Nanostructures: A Manufactured Approach Enabling Application in White Hybrid LEDs," *Journal of Materials Chemistry C* 4 (2016): 5407–5415.

29. L. Illés, M. Sági-Kazár, F. Steinbach, et al., "Fluorescence Lifetime of Plant Leaves with Sub-Nanosecond Resolution," *Measurement Science and Technology* 35 (2024): 085206.

30. G. Landl, T. Langthaler, H. W. Engl, and H. F. Kauffmann, "Distribution of Event Times in Time-Resolved Fluorescence: The Exponential Series Approach—algorithm, Regularization, Analysis," *Journal of Computational Physics* 95 (1991): 1–28.

31. C. Kapnopoulos, E. D. Mekeridis, L. Tzounis, et al., "Fully Gravure Printed Organic Photovoltaic Modules: A Straightforward Process with a High Potential for Large Scale Production," *Solar Energy Materials & Solar Cells* 144 (2016): 724–731.

32. C. Kapnopoulos, A. Zachariadis, E. Mekeridis, et al., "On-the-Fly Short-Pulse R2R Laser Patterning Processes for the Manufacturing of Fully Printed Semitransparent Organic Photovoltaics," *Materials* 15 (2022): 2781.

33. D. J. S. Birch and R. E. Imhof, "Time-Domain Fluorescence Spectroscopy Using Time-Correlated Single-Photon Counting," *Topics in Fluorescence Spectroscopy* 1 (1991): 1–95.

34. D. J. S. Birch and R. E. Imhof, "The Origin of Fluorescence from Trans-Trans Diphenylbutadiene," *Chemical Physics Letters* 88 (1982): 243–247.

18626319, 2026, 8, Downloaded from https://onlinelibrary.wiley.com/doi/10.1002/pssa.202500868 by Cochrane Hungary, Wiley Online Library on [21/04/2026]. See the Terms and Conditions (https://onlinelibrary.wiley.com/terms-and-conditions) on Wiley Online Library for rules of use; OA articles are governed by the applicable Creative Commons License